J Mater Sci (2007) 42:3865–3873
DOI 10.1007/s10853-006-0463-3

Vibration fracture behavior of Sn–9Zn–*x*Cu lead-free solders

Fei-Yi Hung · Truan-Sheng Lui · Li-Hui Chen · Ji-Ge You

Received: 1 September 2005 / Accepted: 17 May 2006 / Published online: 12 February 2007

Abstract The effect of Cu content on the microstructure and the vibration deformation mechanisms of a potential lead-free solder, Sn–9Zn–*x*Cu (x = 0.2, 0.5, 0.7, 1.0 wt.%), are examined in this study. Results show that Zn-rich phase and Sn–Zn eutectic decreased, while Cu–Zn intermetallic compound and proeutectic Sn-rich phase increased with increasing the Cu content. For the specimens with high Cu content (0.7Cu and 1.0Cu), hard massive Cu_5Zn_8 existed mostly amongst the proeutectic Sn-rich phase dendrites, and Zn-rich dispersed unevenly, leading to the deterioration in the tensile strength and ductility. Under a constant vibration force and constant initial-deflection testing, the high Cu specimen with a higher damping capacity was able to absorb more vibration energy and thus possessed a greater vibration fracture resistance. In addition, the lamellar-deformed structures (LDS) and Cu_5Zn_8 were able to increase the crack tortuosity, which in turn increased the crack propagation resistance.

Introduction

The Sn–Zn eutectic alloy has recently been considered as a candidate for a lead-free solder material because of its low melting point (198 °C), excellent mechanical properties and low cost [1, 2]. However, since Zn-containing alloys have the problems of oxidation and wetting [3, 4], new Sn–Zn based alloys are still under development. Many reports have shown that the wetting ability and mechanical properties of Sn–Zn based solders can be enhanced by the addition of Cu, Ag, Bi etc [5–7]. Also, one related study [7] revealed that Cu addition has a significant influence on the oxidation and wetting of Sn–Zn alloys. Considering the low cost of Cu addition, Sn–Zn–Cu alloys show great potential as lead-free solder materials.

Given that failure may occur due to vibration, e.g., in vehicles and aircraft, the vibration fracture resistance should be taken into consideration in the design of Sn–Zn based solder alloys when the solder joints are assembled. Previous studies [8–10] have investigated the vibration behavior of several Sn-based solder alloys under resonant conditions. The eutectic Sn–Zn alloy has been found to exhibit inferior vibration-fracture resistance compared to commonly used Sn–Pb and Sn–Ag solders due to the uniformly distributed Zn needles. Since Cu addition has a significant influence on the microstructure of Sn–Zn alloys, one aim of this study was to use Sn–9Zn–*x*Cu (x = 0, 0.2, 0.5, 0.7, 1.0 wt.%) alloys to investigate the effect of Cu on the resonant vibration fracture behavior. In addition, the crack propagation morphology and the ability to absorb vibration energy were also examined.

F.-Y. Hung (✉) · T.-S. Lui · L.-H. Chen · J.-G. You
Department of Materials Science and Engineering, National Cheng Kung University, Tainan 701, Taiwan, ROC
e-mail: fyhung@mail.mse.ncku.edu.tw
(z7408020@email.ncku.edu.tw)

Experimental procedure

Master alloys of near-eutectic Sn–9Zn–*x*Cu (x = 0, 0.2, 0.5, 0.7, 1.0 wt.%) alloy were prepared by melting pure tin, pure zinc and pure copper in a high-frequency

induction furnace. The alloy ingots were then remelted and cast into a Y-shaped graphite mold. Hereafter, the specimens will be designated according to Cu content as 9Zn, 0.2Cu, 0.5Cu, 0.7Cu, and 1.0Cu (see Table 1). To obtain steady properties, before testing, each specimen was subjected to stabilization treatment at 120 °C for 2 h followed by air cooling to room temperature. The microstructures of the alloys were determined quantitatively using an image analyzer and X-ray diffraction. The Cu-Kα standard (λ = 1.5403 nm) was used for X-ray diffraction. The scanning angle was varied from 25° to 60° and the scanning velocity was 0.5° min^{-1}. The tensile specimens had a gauge length of 20 mm, width of 5.4 mm, and thickness of 2.4 mm. The tensile mechanical properties under an initial strain rate of 7.5×10^{-4} s^{-1}, as well as the hardness of each phase in the matrix, was ascertained.

A simple cantilever beam vibration system was used for the vibration experiments and damping measurements (see Fig. 1a), and test specimens (Fig. 1b), which were rectangular with dimensions $100 \times 20 \times 4$ mm, were mounted and fixed on end to the vibration shaker. Two circular-notches near the clamp were made for observing microstructural evolution in the vicinity of the notch front. The vibration force was monitored using an acceleration sensor (vibration from top to bottom), and the deflection amplitude of the specimens at the end opposite the vibration shaker was measured using a deflection sensor. For the vibration frequency vs. deflection amplitude curve, the maximum deflection amplitude must be at a resonant frequency condition. The resonant frequency was taken as the frequency leading to the largest deflection and was determined by varying the vibration frequency continuously [10].

SEM was used for fracture analysis of the microstructures. Crack tortuosity of the specimens which suffered vibration was quantified. Crack tortuosity is defined as the ratio of the length of the main crack to the projected length of this crack along the transverse direction of the specimen. Each data was the average of 3–4 test results. Damping capacity was measured in terms of logarithmic decrement (δ value), which was derived from the deflection amplitude decay of a specimen under free vibration. Logarithmic decrement value is defined as follows [11]: $\delta = n^{-1} \ln (A_i/A_{i+n})$, where A_i and A_{i+n} are the amplitudes of successive cycles.

Table 1 Chemical composition of the specimens (inductively coupled plasma analysis, ICP)

Specimen	Zn (wt.%)	Cu (wt.%)	Sn (wt.%)
9Zn	9.02	–	Bal.
0.2Cu	9.13	0.22	Bal.
0.5Cu	9.08	0.53	Bal.
0.7Cu	9.11	0.70	Bal.
1.0Cu	8.96	1.01	Bal.

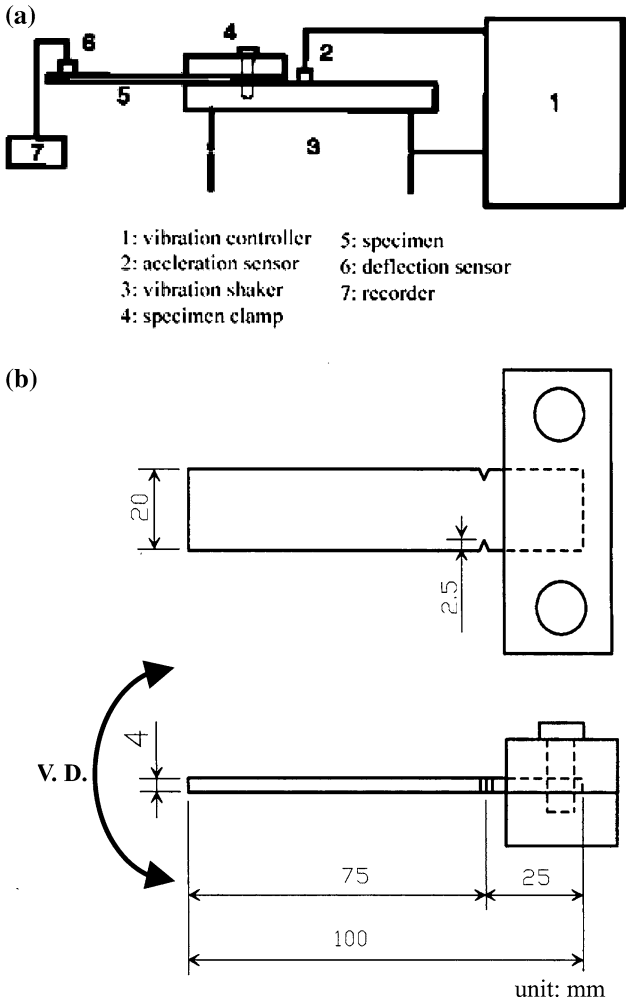

Fig. 1 (**a**) Schematic diagram of the vibration equipment and (**b**) shape and dimensions of the specimens for resonant vibration (Vibration Direction, V.D.)

Results and discussion

Effect of Cu content on the microstructure and the tensile properties

Figure 2 shows the microstructures of the Sn–9Zn–*x*Cu solder alloys. The matrix contained Sn-rich phase, Zn-rich phase, Sn–Zn eutectic and Cu–Zn intermetallics. On increasing the Cu content, Cu–Zn intermetallics and Sn-rich had increased, and Zn-rich and Sn–Zn eutectic decreased. In addition, the finer needle-like Zn-rich phase dispersed in the tin matrix and a very small amount of proeutectic Sn-rich phase and Cu–Zn

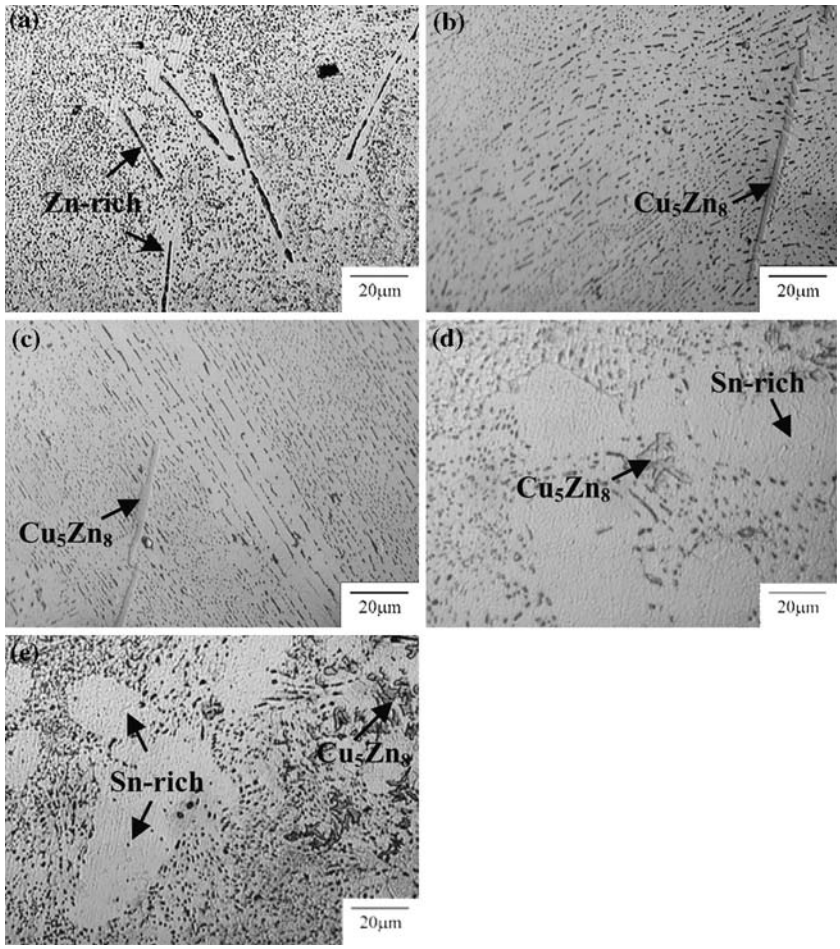

Fig. 2 Microstructure of the Sn–9Zn–*x*Cu solders: (**a**) 9Zn, (**b**) 0.2Cu, (**c**) 0.5Cu, (**d**) 0.7Cu, and (**e**) 1.0Cu

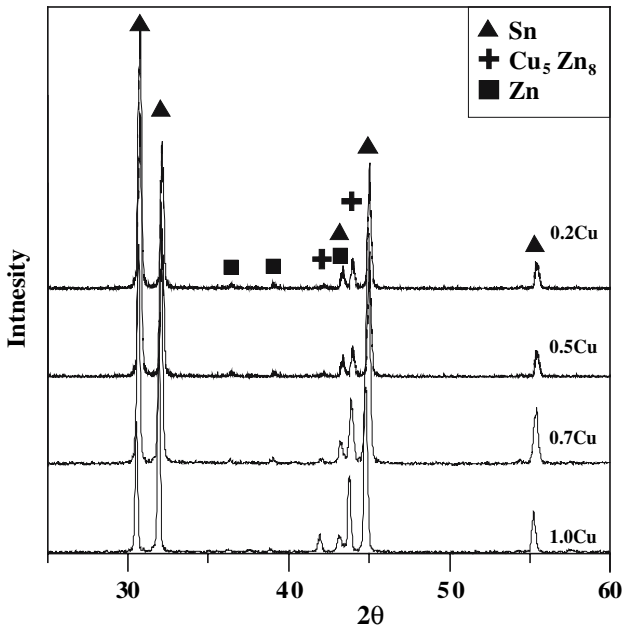

Fig. 3 X-ray diffraction patterns of the Sn–9Zn–*x*Cu solders

intermetallics could be observed in the specimens with lower Cu content (0.2Cu and 0.5Cu specimens). These microstructural features were similar to the Sn–9Zn eutectic. For the specimens with higher Cu content (0.7Cu and 1.0Cu specimens), a great number of proeutectic Sn-rich dendrites formed and Cu–Zn intermetallics existed mostly amongst the proeutectic Sn-rich dendrites.

The X-ray diffraction patterns shown in Fig. 3 identify the Cu–Zn intermetallic phases as Cu_5Zn_8 and the amount of these compounds increased with increasing Cu content. For later discussion, the microhardness of each phase of the 1.0Cu matrix is shown in Fig. 4. The results reveal that the average value for Cu_5Zn_8 compounds was highest, followed by Sn–Zn eutectic and Sn-rich phase, respectively.

Figure 5 shows the typical tensile stress–strain curves of the Sn–9Zn–*x*Cu solder alloys. This figure indicates that the modulus of elasticity of the 0.2Cu specimen was highest, while the specimens with a higher Cu content exhibited a lower modulus of

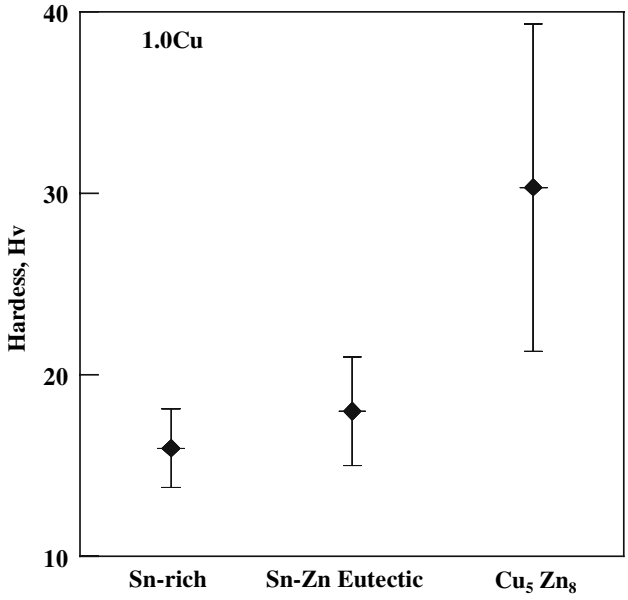

Fig. 4 Micro-hardness of each phase for the 1.0Cu specimen

elasticity. Detailed tensile results (Fig. 6) revealed that the 0.2Cu specimen possessed higher tensile strength and lower total elongation than the other specimens. As for the total elongation, all Sn–9Zn–*x*Cu specimens were higher than 40%.

In the structures of the lower Cu content specimens (Fig. 2b, c), a large amount of Zn-rich phase dispersed in the tin matrix and resulted in an increase in the area of the phase boundaries. This not only made it harder for the dislocation to move, but also led to better dispersion strengthening. This must be one reason why

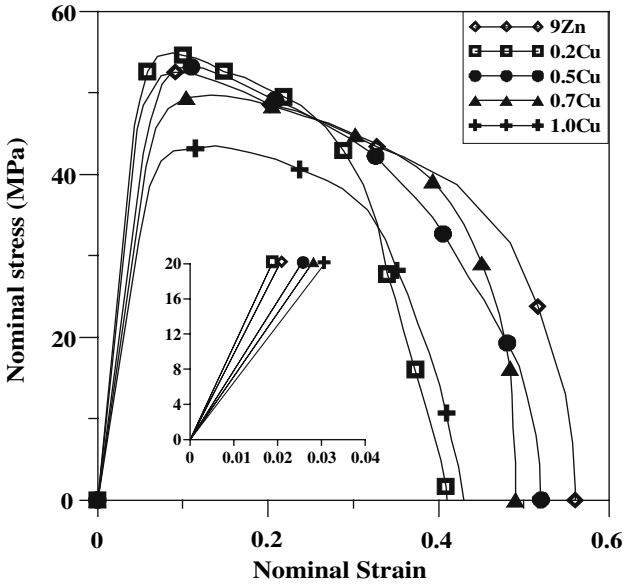

Fig. 5 Engineering stress–strain curve of the Sn–9Zn–*x*Cu specimens

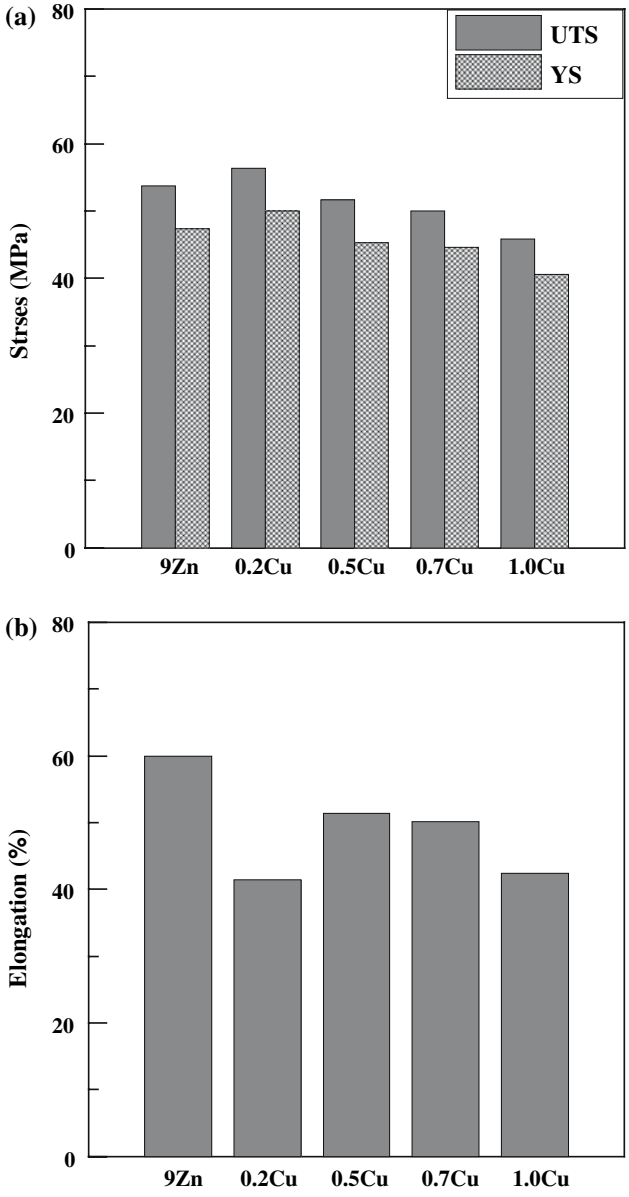

Fig. 6 Tensile mechanical properties of the specimens: (**a**) U.T.S. and Y.S., (**b**) total elongation

the tensile strength was raised. When a further 0.7 wt.% Cu was added into the Sn–9Zn–*x*Cu alloy (Fig. 2d, e), the number of proeutectic Sn-rich dendrites increased greatly, Sn–Zn eutectic decreased and Zn-rich phase dispersed unevenly, leading to a deterioration in the tensile strength. Notably, Sn-rich phase in the structure increased with an increased Cu content, which should have improved the ductility. However, the experimental results reveal that both the ductility and tensile strength of the higher Cu content specimens were lower. This is because the amount of hard massive Cu_5Zn_8 compounds (Fig. 4) increased with an increased Cu content, and existed mostly

Table 2 Logarithmic decrement (δ value) and resonant frequency (fixed vibration force: 3.5G, G: 9.8 m/s^2) of the Sn–Zn–x Cu specimens

Specimen	(value	Frequency (Hz)
9Zn	0.228	82 ± 1
0.2Cu	0.178	83 ± 1
0.5Cu	0.224	83 ± 1
0.7Cu	0.293	76 ± 1
1.0Cu	0.311	76 ± 1

amongst the proeutectic Sn-rich dendrites. Cu_5Zn_8 compounds undermined the ductility of Sn-rich phase. So, Cu addition resulted in variations in the structure, which in turn affected the tensile data.

D–N curve characteristic and vibration life of Sn–9Zn–xCu alloy

Table 2 shows the logarithmic decrement value (δ) of the Sn–9Zn–xCu alloys. The 0.2Cu specimen possessed the lowest δ value, showing that it had the lowest damping capacity. When the Cu content of the specimen exceeded 0.7 wt.%, the logarithmic decrement value exhibited an obvious upward trend (see Table 2, comparing x.x Cu specimen with 9Zn specimen). In addition, the resonant frequencies of the Sn–9Zn–xCu specimen under a fixed vibration force of 3.5G are also shown in Table 2. The specimens with lower Cu content (0.2Cu and 0.5Cu specimens) had similar resonant frequencies (~83 ± 1 Hz). However, the resonant frequency of the 0.7Cu and 1.0Cu specimens were lower (~76 ± 1 Hz) than that of the other specimens.

Figure 7a shows the D–N curves (deflection amplitude vs. number of vibration cycles) of the specimens under resonant frequency. This figure shows that the initial deflection amplitude of the 0.2Cu specimen was highest (~1.8 mm), while that of the 1.0Cu specimen was lowest (~1.2 mm). Comparing the initial deflection amplitudes of Fig. 7a with the logarithmic decrement values (δ) of Table 2, we see that the initial deflection amplitude of the specimens was inversely related to the Cu content. In other words, the specimens with higher δ value possessed a lower initial deflection amplitude. Figure 7a, as well as relevant references [8–10], indicates that the D–N curve can be divided into an initial stage with ascending deflection amplitude, a second stage in which deflection remained constant, and a final stage with a descending deflection amplitude. The ascending and constant deflection amplitudes within Stage I and Stage II can be attributed to the effect of strain hardening in competition with crack generation and linking within this region. The descending deflection amplitude in Stage III is due to the deviation of the actual vibration frequency from the resonant frequency caused by the inward propagation of major cracks. In Fig. 7a, the 0.2Cu curve shows an obvious Stage I, revealing that strain hardening was active during initial vibration. There is a virtual absence of Stage II, and the 0.2Cu curve immediately enters Stage III. As for the 0.7Cu and1.0Cu curves, they begin from Stage II, where they remain for an extended period, before finally entering Stage III.

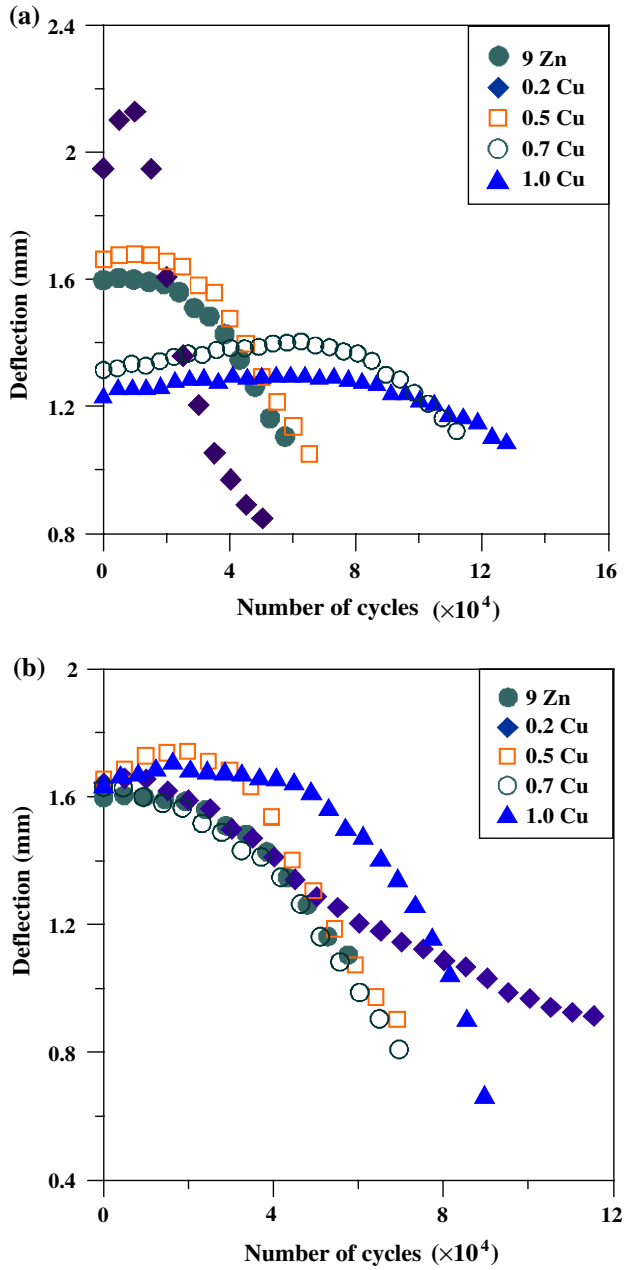

Fig. 7 D–N curves of the Sn–9Zn–xCu specimens: (**a**) under a fixed vibration force of 3.5G and (**b**) under a fixed initial deflection amplitude of 1.6 mm

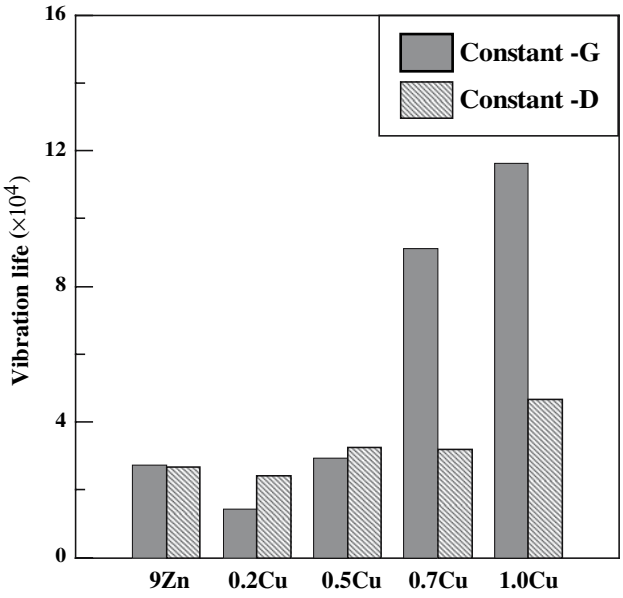

Fig. 8 Vibration life of the Sn–9Zn–*x*Cu solders

To avoid the effect of damping capacity, in this study the vibration force of the specimens was controlled to obtain identical initial deflection amplitude. This allowed us to measure the variation of the D–N curves under constant vibration strain conditions (i.e., identical initial deflection conditions). Under the initial deflection of 1.6 mm, the D–N curves of the specimens were similar (Fig. 7b). Comparing Fig. 7a with Fig. 7b, the vibration cycle number of the 0.2Cu specimen increased within Stage II and Stage III due to the initial deflection amplitude descending (from 1.96 to 1.60 mm). However, when the initial deflection amplitude was raised in the 0.7Cu and 1.0Cu specimens, the number of vibration cycles decreased significantly within Stage II and Stage III.

A previous study revealed that a Sn–9Zn–0.5Cu specimen had a ~3 Hz deviation of the actual vibration frequency from the resonant frequency when the deflection amplitude was decreased to 94% of the maximum value. Therefore, the vibration life in this study was defined as the vibration cycle number when the deflection amplitude was reduced to 95% of the maximum value at the beginning of Stage III. Based on this definition, Fig. 8 shows the critical number of vibration cycles. We see that the vibration life under constant force (-G) conditions lengthened with a higher Cu content. In addition, the vibration life of

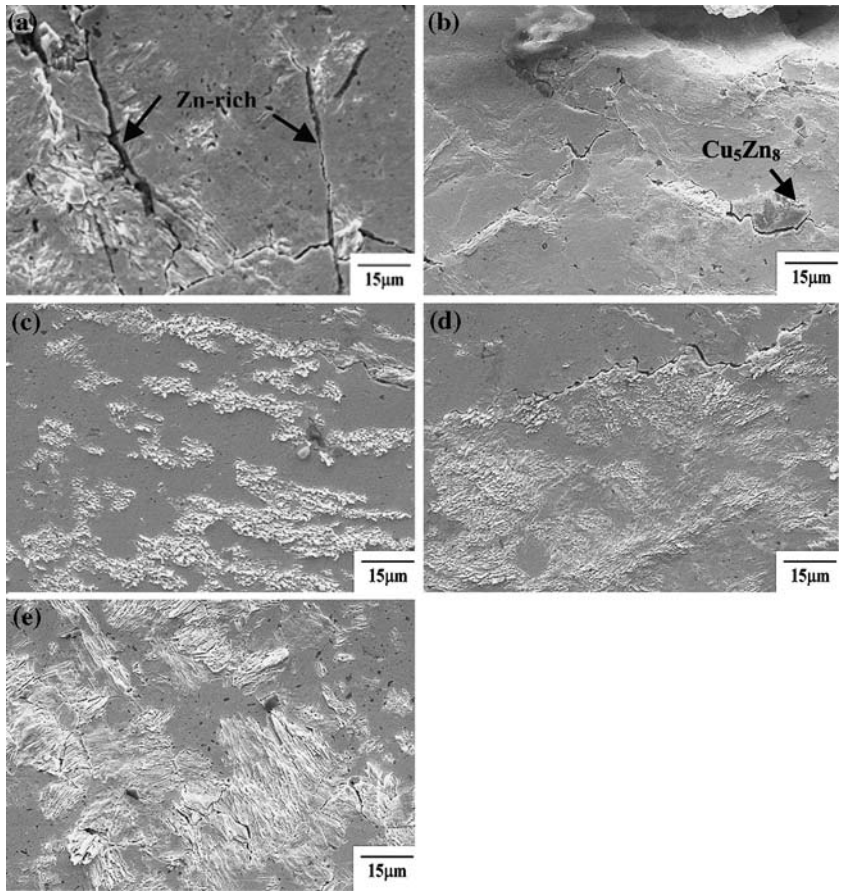

Fig. 9 Vibration deformed structures of Sn–9Zn–*x*Cu specimens (3.5G): (**a**) 9Zn, (**b**) 0.2Cu, (**c**) 0.5Cu, (**d**) 0.7Cu, and (**e**) 1.0 Cu

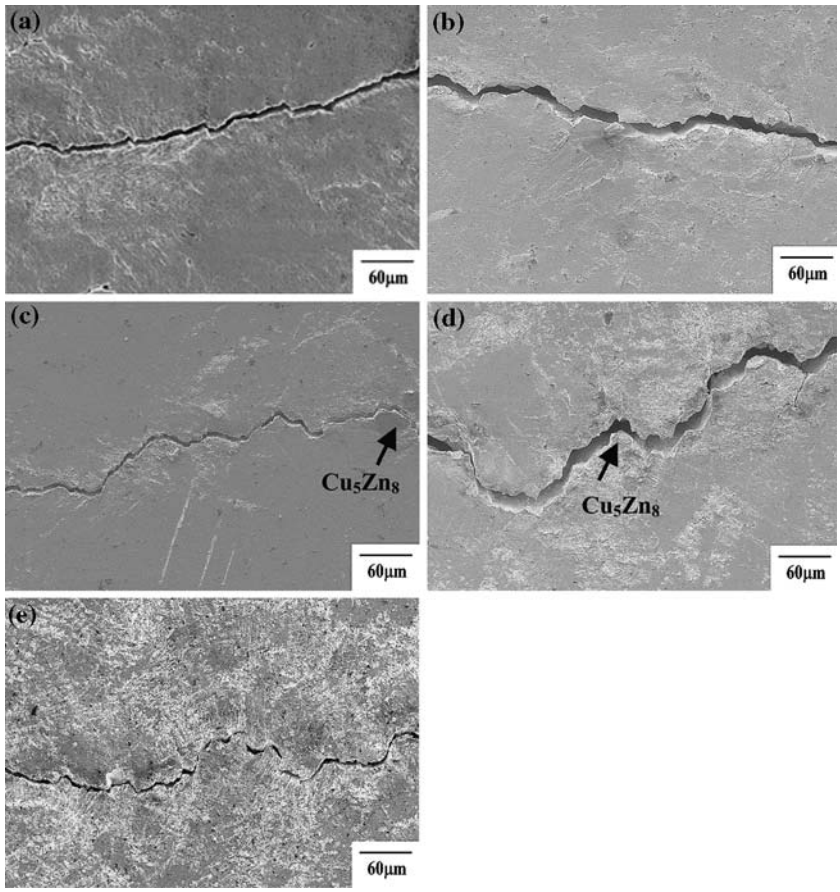

Fig. 10 Surface morphology of the Sn–9Zn–*x*Cu specimens after vibration (3.5G): (**a**) 9Zn, (**b**) 0.2Cu, (**c**) 0.5Cu, (**d**) 0.7Cu, and (**e**) 1.0 Cu

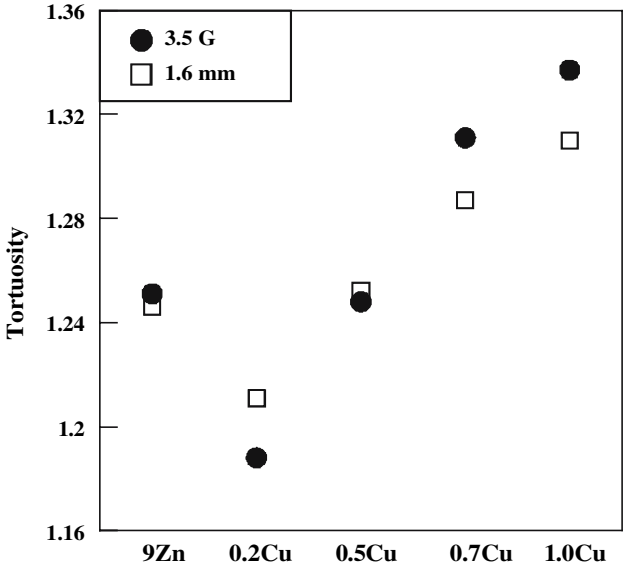

Fig. 11 The crack tortuosity of the Sn–9Zn–*x*Cu under both constant force (3.5G) and initial-deflection condition (1.6 mm)

the 1.0Cu specimen was better, while those of the other specimens were similar under the identical initial deflection of 1.6 mm (-D). Under both constant force and initial-deflection conditions, the specimens with a higher damping capacity exhibited a greater vibration fracture resistance.

Under constant force condition (3.5G), the specimens with higher Cu content possessed a lower initial deflection (Fig. 7a) and a higher logarithmic decrement value (Table 2). Our results confirm that these specimens underwent a lower vibration strain which reduced the driving force of crack propagation. This is one reason why the higher Cu specimens possessed a higher vibration life. However, the higher modulus of elasticity of the lower Cu specimens (see Fig. 5a, i.e., rigidity) not only raised the deflection, but also reduced the logarithmic decrement value, detrimentally affecting the crack propagation resistance and the vibration life. SEM was used in this study to examine the characteristics and mechanisms of vibration fracture.

Effects of vibration-deformed structure and proeutectic second-phase on the vibration fracture behavior

The surface lamellar-deformed structures (LDS) of all specimens were observed after the constant-force

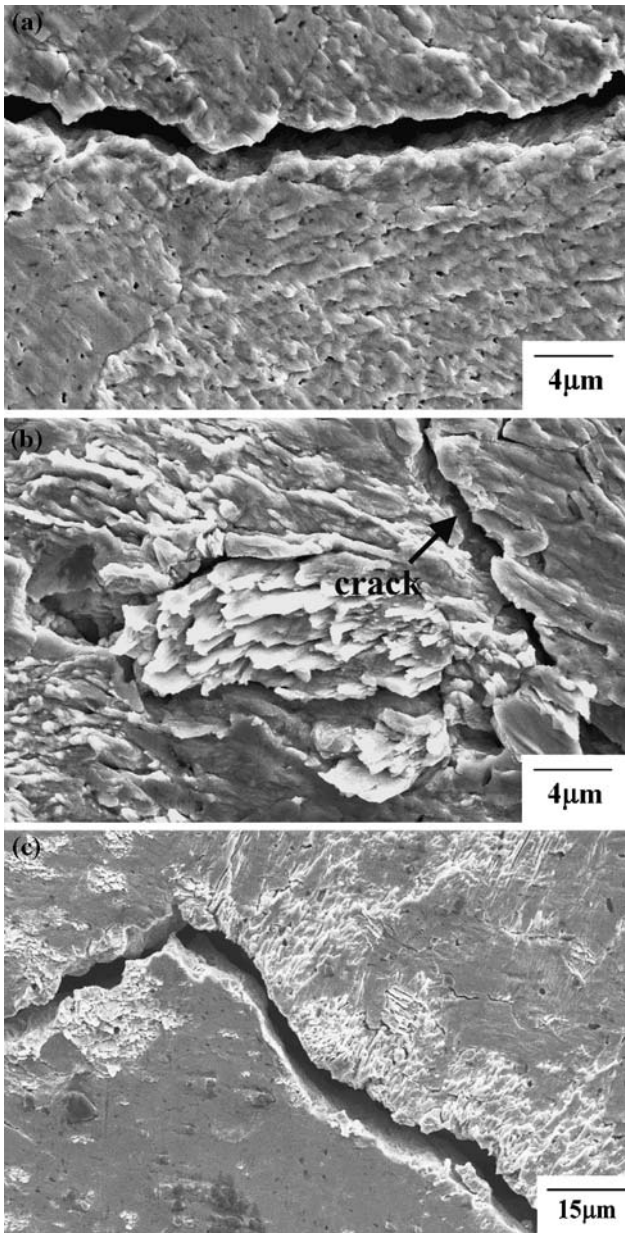

Fig. 12 Vibration deformed structures of the Sn–9Zn–*x*Cu specimens (3.5G): (**a**) 0.2 Cu, (**b**) 1.0 Cu, and (**c**) lamellar deformed structures enhanced the tortuosity (1.0Cu)

vibration test (Fig. 9). The lamellar-deformation regions were mostly found in the Sn–Zn eutectic structure of the 9Zn specimen (Fig. 9a). As for the lower Cu content specimens, lamellar-deformed structures (LDS) were found not only in the eutectic structure, but also in the proeutectic Sn-rich phase (Fig. 9b,c). Notably, the area fraction of LDS increased as the Cu content of a specimen increased (Fig. 9d,e). From observations of the crack propagation, it was found that the regions of LDS by the side of a vibration-crack also had a tendency to expand with increasing the Cu content of a specimen. In addition, the higher Cu specimens had a higher crack tortuosity than that of the lower Cu specimens (Fig. 10), revealing that crack tortuosity is closely related to the vibration-deformed characteristics.

Figure 11 shows the crack tortuosity of the Sn–9Zn–*x*Cu specimens after both constant force (3.5G) and initial-deflection (1.6 mm) vibration testing. Regardless of constant force or constant initial-deflection testing, the tortuosity of the 1.0Cu specimen was higher and that of the 0.2Cu specimen was lower. This result agrees with the δ value of Table 2. In addition, Fig. 11 also explain that even increasing the vibration force of the high Cu content specimen made the initial-deflection increase (from ~1.3 mm (Fig. 7a) to ~1.6 mm (Fig. 7b), and this still possessed higher crack tortuosity. In other words, the high Cu content specimen had excellent crack propagation resistance.

Reportedly [1, 8–10], the lamellar-deformed structures (LDS) of proeutectic Sn-rich phase also affect the damping capacity. The high Cu content specimen was a hypoeutectic structure (Fig. 2d, e), within which could be found a great number of LDS on the proeutectic Sn-rich phase after vibration testing. These LDSs (Fig. 9d, e) not only absorbed the vibration energy, but also reduced the deflection, which was advantageous to crack propagation resistance. However, the lower Cu content matrix was similar to the Sn–9Zn eutectic structure (Fig. 2b, c) and Zn-rich phase suppressed the formation of LDS (Fig. 9b, c), which in turn reduced both the absorbability of the vibration energy and vibration life deterioration. After vibration testing, the micro-cracks near the regions of LDS also had a tendency to increase with increasing the Cu content of a specimen (Fig. 12a, b). The vibration micro-cracks led the major crack to propagate along the regions of LDS and increased the crack tortuosity (Fig. 12c). This must be one reason for the high Cu content specimen having higher crack tortuosity.

In Fig. 10c, d, Cu_5Zn_8 is separated from the boundary of the lamellar-deformed zone on the crack propagation path, and micro-cracks were also observed around this Cu_5Zn_8 (Fig. 9b). These finds also explain why the crack tortuosity was raised. So, the proeutectic Cu_5Zn_8 was advantageous to vibration resistance. Detailed observations of the crack propagation path (Figs. 9a, 10a) reveal that the main crack mostly grew along needle-like Zn-rich phase without breaking it, while a few lamellar-deformed zones and micro-cracks were found. That is why the crack tortuosity was lower. According to relevant references [12–13], the internal friction effect between the second phase and matrix affects the damping capacity of the material. In this

study, Cu_5Zn_8 compounds increased and Zn-rich phase decreased with increasing the Cu content of a specimen. From observations of the vibration-deformed characteristic and Fig. 8, the hard massive Cu_5Zn_8 compound (Fig. 4) was able to provide a greater vibration resistance than Zn-rich phase. Both lamellar-deformed structures (LDS) and proeutectic second phase were the main factors in the vibration crack propagation mechanism.

Conclusion

1. For Sn–Zn–*x*Cu solder alloys, Sn-rich phase and Cu–Zn intermetallics increased, and Zn-rich phase and Sn–Zn eutectic decreased with increasing Cu content. In the specimens with higher Cu content (0.7Cu and 1.0Cu specimens), the tensile strength deteriorated owing to the hard massive Cu_5Zn_8 existing mostly amongst the Sn-rich dendrites and Zn-rich dispersing unevenly.
2. When the Cu content of a specimen exceeded 0.7 wt.%, the logarithmic decrement value increased and the modulus of elasticity dropped. The resultant higher damping capacity was able to absorb more vibration energy and lengthen the vibration life. In addition, the crack tortuosity and the amount of LDS were raised with increasing the Cu content. The proeutectic Cu_5Zn_8 not only increased the crack tortuosity but was also advantageous to vibration resistance.

Acknowledgements The authors are grateful to the Chinese National Science Council for its financial support (Contract: NSC 94-2216-E-006-008).

References

1. Song JM, Lan GF, Lui TS, Chen LH (2003) Scr Mater 48:1047
2. Wu CML, Law CMT, Yu DQ, Wang L (2003) J Electron Mater 32:63
3. Hua F, Glazer J (1997) Proceeding of the TMS annual meeting on design and reliability of solders and solder interconnections, p 65
4. Vaynman S, Fine ME (1999) Scr Mater 41:1269
5. Chang TC, Wang MC, Hon MH (2004) J Crystal Growth 263:223
6. Kim KS, Kim KS, Hwang CW, Suganuma K (2003) J Alloys Comp 352:273
7. Yu DQ, Xie HP, Wang L (2004) J J Alloys Comp 385:119
8. Chung CM, Lui TS, Chen LH (2004) Mater Trans 42:2064
9. Chung CM, Lui TS, Chen LH (2001) J Mater Res 16:2644
10. Chung CM, Lui TS, Chen LH (2001) J Electron Mater 30:1232
11. Steidel RF Jr (1989) An introduction to mechanical vibration, 3rd edn. Wiley, p 169
12. Perez RJ, Zhang J, Gungor MN, Lavernia EJ (1993) Metall Trans 24A:701
13. Okabe M, Mori T, Mura T (1981) Phil Mag A 44:1